Wideband Inverse Matrix for Radiated Two-Stage MIMO Measurements

Jun Li, *Student Member, IEEE*, Bin Lin, *Senior Member, IEEE*, Yihong Qi, *Fellow, IEEE*, James L. Drewniak, *Fellow, IEEE*, Jiang Zhu, *Fellow, IEEE*, and Daryl G. Beetner, *Senior Member, IEEE*

***Abstract*— Multiple-input and multiple-output (MIMO) technology is one of the significant components in the growing fifth-generation (5G) communication systems. The 5G system has expanded its frequency range and widened the bandwidth to achieve higher throughput rates and more stable wireless qualities, which brings new challenges to the over-the-air (OTA) MIMO evaluations. The wide bandwidth introduces systematic uncertainties into the MIMO measurement because of the increased amplitude and phase variation issues under different frequencies in the wideband signals, and it could lead to valid MIMO throughput measurement results when severe. The effect on antenna isolation resulting from amplitude and phase variation in wideband MIMO measurements is analyzed based on the radiated two-stage (RTS) MIMO measurement method. A wideband inverse matrix algorithm is introduced to solve this issue and improve the wideband MIMO antenna isolation. The proposed method can be used in both multiple probe anechoic chamber (MPAC) and RTS chambers, which paves the way for decreasing the OTA measurement uncertainties on both 5G sub-6-GHz wideband MIMO and millimeter-wave MIMO evaluations.**

***Index Terms*— Multiple-input and multiple-output (MIMO), over the air (OTA), radiated two-stage (RTS), wideband inverse matrix.**

I. Introduction

THE fifth-generation (5G) communication technology brings a new Internet of Things (IoT) revolution, enabling more advanced communication quality with higher throughput rates and lower latency, and reducing communication costs for wireless terminals. According to global system for mobile communications associations (GSMA's) forecast, the number of global IoT devices will reach approximately 24.6 billion in 2025, and the applications of IoT devices will continue to achieve explosive growth under the gradual maturation of 5G technologies [1]. In addition, multiple-input and multiple-output (MIMO) technology, with higher and more stable throughput rates, becomes one of the significant features in 5G systems to improve the user experience, which also brings new challenges for MIMO system evaluation in research and development (R&D), certification, and production line testing before they can be marketed.

As the 3rd-Generation Partnership Project (3GPP) and Cellular Telecommunication and Internet Association (CTIA) defined, there are strict requirements for the accuracy, stability, and consistency of the overall wireless performance of over-the-air (OTA) testing for wireless performance evaluation [2], [3], and the measurement methods should also be applicable for 5G and beyond communication system measurements. There are two standard MIMO OTA methods specified: radiated two-stage (RTS) method and the multiple probe anechoic chamber (MPAC) method [4], [5], and the primary evaluation metric is the throughput rate. These two methods provide a reliable method for MIMO performance evaluation and means of uncertainty verification and design optimization, which have been widely applied to the 4G long-term-evolution (LTE) MIMO OTA evaluation. The methods simulate a specified electromagnetic propagation environment in an anechoic chamber and test throughput rates under the defined channel models.

However, with the increased frequency bandwidth and more complex radio frequency (RF) components in 5G system design, the amplitude and phase variation issue under different frequencies in communication links introduces significant challenges and results in uncertainty in MIMO OTA evaluations. When conducting 4G MIMO measurements, the testing signals are narrowband ($\leq$20 MHz), so the amplitude and phase variation issues are neglected because the amplitude and phase in the frequency band are almost identical to the center frequency. However, in 5G wideband MIMO measurements, the variation of amplitude and phase in the frequency band, especially the phase variations, must be considered in MIMO measurement methods; otherwise, measurement uncertainties can be introduced in 5G MIMO evaluations in both MPAC and RTS methods.

In the RTS MIMO measurement method, an "Inverse Matrix" is introduced for canceling the spatial transmission matrix, realizing a "Direct Connection" between the base station emulator (BSE) and receivers of the device under

Manuscript received 11 November 2022; revised 3 March 2023; accepted 27 April 2023. Date of publication 19 May 2023; date of current version 4 August 2023. This work was supported by the National Natural Science Foundation of China under Grant 61971083 and Grant 51939001. *(Corresponding author: Bin Lin.)*

Jun Li is with the College of Information and Communication Engineering, Dalian Maritime University, Dalian 116026, China, and also with General Test Systems Inc., Shenzhen 518000, China (e-mail: jun.li@generaltest.com).

Bin Lin is with the College of Information and Communication Engineering, Dalian Maritime University, Dalian 116026, China, and also with the Network Communication Research Centre, Peng Cheng Laboratory, Shenzhen 518052, China (e-mail: binlin@dlmu.edu.cn).

Yihong Qi is with the College of Information and Communication Engineering, Dalian Maritime University, Dalian 116026, China, and also with the Peng Cheng Laboratory, Shenzhen 518000, China (e-mail: qiyh@pcl.ac.cn).

James L. Drewniak and Daryl G. Beetner are with the EMC Laboratory, Missouri University of Science and Technology, Rolla, MO 65409 USA (e-mail: drewniak@mst.edu; daryl@mst.edu).

Jiang Zhu is with the Meta Reality Labs, Sunnyvale, CA 94010 USA (e-mail: jiangzhu@ieee.org).

Color versions of one or more figures in this article are available at https://doi.org/10.1109/TAP.2023.3276443.

Digital Object Identifier 10.1109/TAP.2023.3276443

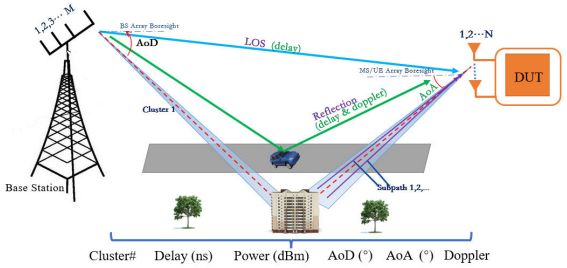

Fig. 1. Overview of a MIMO channel model.

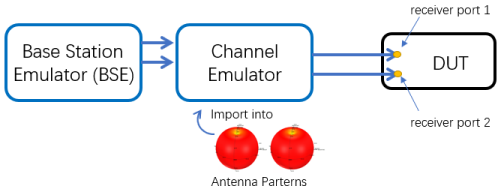

Fig. 2. Conducted 2 × 2 MIMO measurement.

test (DUT). In a real-world environment, the spatially cross-transmitted signals cannot be eliminated by the inverse matrix, so antenna isolation is defined to describe the magnitude relationship between the crossed signals and the desired signals [6], [7]. Antenna isolation is a measurement uncertainty-related parameter for OTA MIMO evaluations. Antenna isolation greater than 20 dB is achievable for LTE MIMO measurements for a 20-MHz bandwidth. However, with the increased bandwidth in 5G systems (FR1 with 100 MHz and FR2 with 400 MHz), the calculated inverse matrix cannot be fully adapted to all the wide frequency bands because of the dramatic variation of amplitude and phase. Thus the "Direct Connection" in the test environment is challenging to achieve, and the antenna isolation is significantly reduced, thus resulting in high measurement uncertainties in RTS MIMO measurements, and even failing to evaluate the actual wireless performance of the DUT.

This article analyzes and verifies the effects of amplitude and phase variations in wideband signals on MIMO antenna isolation. Also, engineering issues to be considered in the MIMO chamber design are proposed, and a wideband inverse matrix algorithm is analyzed and realized to solve the wideband MIMO antenna isolation. Finally, experiments are performed to verify the effectiveness of the wideband inverse matrix algorithm on antenna isolation in RTS MIMO evaluations. This article is organized into five main parts. At first, the theory of MIMO measurement based on the standard RTS method is introduced in Section II. The wideband effects on RTS MIMO evaluation are analyzed in Section III, and the principles of solutions and realizations are explained in Section IV. Finally, the verifications and experimental results are shown in Section V and followed by the conclusion.

II. RTS Method Introduction

The channel models in OTA MIMO measurement are introduced in this section, and the principle of the RTS MIMO evaluation is briefly described. The importance of antenna isolation in MIMO measurement is elaborated herein.

A. MIMO Channel Modeling

MIMO OTA testing is the simulation of the channel model defined in 3GPP to represent the complex electromagnetic propagation environment. As shown in Fig. 1, the base station has M transmitting antennas, and the DUT has N receiving antennas. The basic parameters for each transmission link in this channel model include the number of clusters, the antenna patterns of the wireless terminals and the base station, the Doppler effects, the time delay, and the power distribution, as well as the angle of departure (AoD) and the angle of arrival (AoA) [8]. The channel model between the mth transmitting antenna in the base station and the nth receiving antenna in DUT is described as [8]

$$h_{n,m}(t) = \sum_{l=1}^{L} e^{(j2\pi\Phi_l t + \Psi_l + (-j2\pi f \tau_l))} \begin{bmatrix} G^{V}_{n,DUT}(\alpha_{l,AOA}) \\ G^{H}_{n,DUT}(\alpha_{l,AOA}) \end{bmatrix}^{T} \times \begin{bmatrix} \chi_l^{V,V} & \chi_l^{V,H} \\ \chi_l^{H,V} & \chi_l^{H,H} \end{bmatrix} \times \begin{bmatrix} G^{H}_{m,BS}(\beta_{l,AOD}) \\ G^{H}_{m,BS}(\beta_{l,AOD}) \end{bmatrix} \quad (1)$$

where l is one of the L subpaths; t and f are the time and tested center frequency, respectively; ψ_l, Φ_l, and τ_l are the prime phase, Doppler effect, and the time delay of the lth subpath, respectively; $G^{x}_{n,DUT}$ and $G^{x}_{m,BS}$ (x representing the polarization) are the antenna gains of the nth receiving antenna and the mth transmitting antenna, and $\alpha_{l,AoA}$, $\beta_{l,AoD}$, and $\chi_l^{x,y}$ are the AoA, the AoD, and the path loss from antenna polarization y to x in the lth subpath.

In traditional 2 × 2 MIMO measurements, as shown in Fig. 2, the testing signals (the channel models and antenna patterns are integrated) are transmitted from the channel emulator to receiver ports of the DUT using cables. However, desensitivity issues and high cable isolation result in measurement inconsistencies with real usage applications, which can lead to MIMO evaluation failure [9], [10], [11].

B. RTS Method for MIMO OTA Measurements

The RTS MIMO measurement method is one of the standard OTA MIMO evaluation methods [4], [5], which is implemented through both mathematical and physical realization. The RTS method is divided into two distinct stages. The first stage is to obtain the receiving antenna patterns of each antenna, and transmitting matrix H between the transmitting ports of the base station and receiving ports of the DUT. The second stage is to calculate and apply the inverse matrix M to the channel emulator to perform the throughput measurement process. The second stage can be realized in an instrument based on the mathematical theory and RF components, such as an amplifier, attenuator, and phase shifter.

As shown in Fig. 2, the testing signals with channel models are delivered to receivers OTA, and the communication links exist in each transmitting antenna and each receiver [12]. For an N × N system, the relationships between transmitting

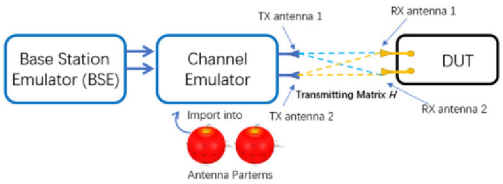

Fig. 3. Communication link in a 2 × 2 OTA MIMO measurement.

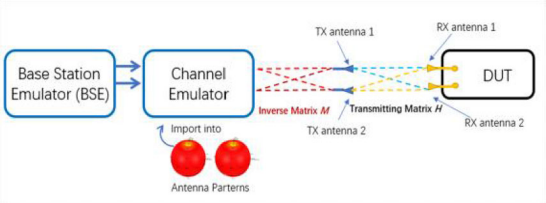

Fig. 4. Inverse matrix M in a 2 × 2 OTA MIMO measurement.

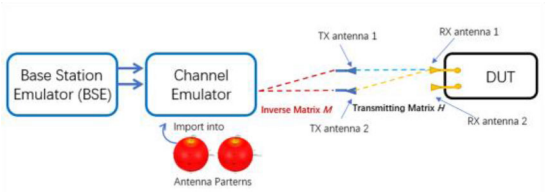

Fig. 5. Transmitting signal 2 to receiver 1 of the DUT.

antennas and receivers are written as

$$y(t) = H(t) * x(t) \tag{2}$$

where the received signals $(y_1, y_2, \ldots, y_N)$ are a function of the transmitting signals $(x_1, x_2, \ldots, x_N)$, and the total transmitting matrix H is defined as

$$H(t) = \begin{bmatrix} h_{1,1}(t) & \cdots & h_{1,N}(t) \\ \vdots & \ddots & \vdots \\ h_{N,1}(t) & \cdots & h_{N,N}(t) \end{bmatrix}. \tag{3}$$

For the 2 × 2 MIMO OTA measurement shown in Fig. 3, the desired signals for each receiving port cannot be delivered to each receiver correctly because of the cross signal transmission from Tx antenna 1 to Rx antenna 2, and from Tx antenna 2 to Rx antenna 1. The transmitting matrix H in 2 × 2 MIMO environment is then

$$H_{2\times2}(t) = \begin{bmatrix} h_{1,1}(t) & h_{1,2}(t) \\ h_{2,1}(t) & h_{2,2}(t) \end{bmatrix}. \tag{4}$$

In order to eliminate the cross signal transmission in MIMO OTA measurements, an inverse matrix M is used to eliminate the effects of cross-transfer and realize a "Direct Connection" between the transmitting signals to receivers. The inverse matrix M in an $N \times N$ system is

$$M(t) = \begin{bmatrix} m_{1,1}(t) & \cdots & m_{1,N}(t) \\ \vdots & \ddots & \vdots \\ m_{N,1}(t) & \ldots & m_{N,N}(t) \end{bmatrix} \tag{5}$$

after applying the inverse matrix M, the relationship between transmitting signals to receivers in (2) is modified as

$$y(t) = [M(t) \times H(t)] * x(t). \tag{6}$$

As shown in Fig. 4, the total transmitting matrix T for a 2 × 2 MIMO system is then

$$T = \begin{bmatrix} t_{11} & t_{12} \\ t_{21} & t_{22} \end{bmatrix} = \left[M_{2\times2}(t) \times H_{2\times2}(t)\right] = \begin{bmatrix} m_{11} & m_{12} \\ m_{21} & m_{22} \end{bmatrix} \times \begin{bmatrix} h_{11} & h_{12} \\ h_{21} & h_{22} \end{bmatrix}. \tag{7}$$

In the ideal case, the total transmitting matrix T is an identity matrix, i.e., $t_{11} = t_{22} = 1$ and $t_{12} = t_{21} = 0$. Therefore, the testing signals from transmitting signals 1 and 2 are delivered to receivers 1 and 2, respectively. The cross signals are eliminated after applying the inverse matrix M. However, in practice, the cross signals are not entirely eliminated due to the reflection in the chamber and the limited accuracy of the amplifier, attenuator, and phase shifter. To evaluate the impact of the cross signals for MIMO measurement, the concept of antenna isolation is defined as

$$\begin{aligned} Ios_1 &= 20log_{10}|t_{11}/t_{12}| \\ Ios_2 &= 20log_{10}|t_{22}/t_{21}| \\ Ios_t &= \min(Ios_1, Ios_2) \end{aligned} \tag{8}$$

where Ios_1 and Ios_2 represent the ratio (in dB) of the desired signal to cross signal of receiving antennas 1 and 2, respectively, and the Ios_t is the system isolation for a 2 × 2 MIMO system.

In RTS MIMO testing, antenna isolation is a significant factor related to MIMO measurement uncertainty and is affected by the position and the receiving antenna patterns of the DUT, as well as the transmitting antennas. In addition, the differences in free-space path loss (FSPL) and antenna directivity/pattern are reflected in the transmission matrix H. However, once the inverse matrix is calculated and loaded, these differences are eliminated. As long as the antenna isolation requirements are met, the FSPL and antenna directivity/pattern will not have an impact on the test results. To ensure lower uncertainty for RTS MIMO [13], [14], [15] measurements, the isolation must be greater than 15 dB before throughput measurements [16] to achieve a satisfactory "Direct Connection." After applying the inverse matrix and achieving sufficient antenna isolation, the MIMO throughput measurement can be performed to evaluate the MIMO performance of the DUT [17], [18], [19].

III. Wideband MIMO Measurement Analysis Based on the RTS Method

As indicated in (7) and Fig. 4, the matrix T should be nearly the identity matrix, which means that the transmitting signals 1 and 2 are directly delivered to receiver 1 and receiver 2, respectively, without cross-transmission. As an example, the communication link from transmitting signal 2 to receiver 1 is shown in Fig. 5. After applying the inverse matrix M in a 2 × 2 MIMO measurement, the two paths from transmitting signal 2 to receiver 1 are not expected to exist. By adjusting the amplitude and phase in the inverse matrix, these two path

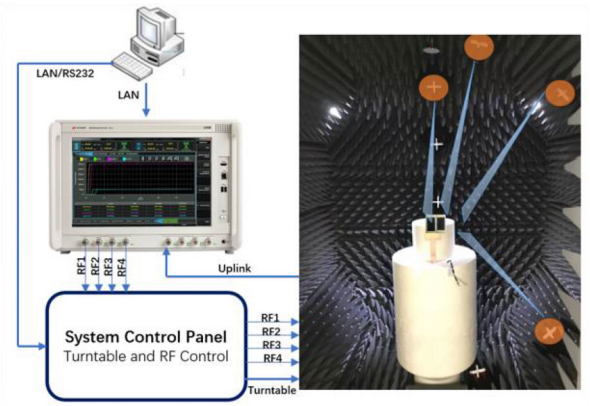

Fig. 6. Schematic for MIMO measurement chamber.

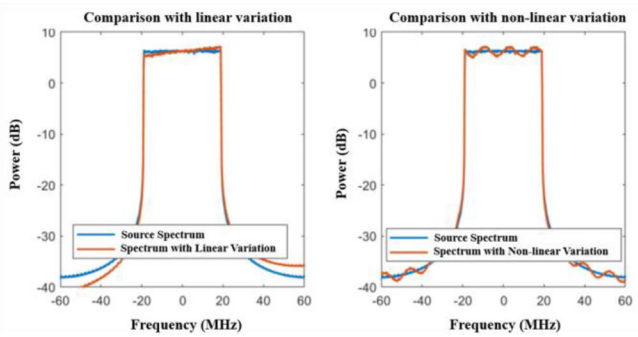

Fig. 7. Two basic cases: linear functional variation and nonlinear functional variation.

TABLE I
MAXIMUM AMPLITUDE VARIATION FOR MIMO MEASUREMENT FOR DIFFERENT BANDWIDTHS

Bandwidth (MHz)	Maximum Variation (dB)
20	4.0
40	2.1
50	1.8
60	1.4
80	1.1
90	1.0
100	0.8

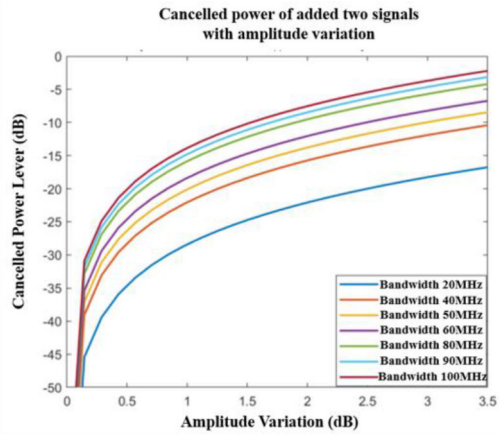

Fig. 8. Canceled power level under a different bandwidth and amplitude variation.

signals will have the same amplitude and opposite phase (180° difference) when arriving at receiver 1. Then, the transmitting signal 2 is eliminated in receiver 1 to ensure sufficient isolation in (8) for MIMO measurements.

The inverse matrix M is implemented with amplifiers, attenuators, and phase shifters [or digital signal processing (DSP) modules and field programmable gate array (FPGA)] in the channel emulator, which is widely used in 4G LTE MIMO measurements with signal bandwidth less than 20 MHz. The variation of amplitude and phase is not apparent when the signal bandwidth is narrow, i.e., in this range, so signal cancellation is implemented based on the center frequency to realize high isolation.

However, when it comes to MIMO testing of the 5G sub-6-GHz band, with a maximum bandwidth of 100 MHz in a single carrier, the inverse matrix M is difficult to realize adequately over the entire frequency band because of the significant variation in amplitude and phase in the wideband signals, which is ignored in narrowband MIMO testing. As shown in Fig. 5, these two signal paths are not sufficiently eliminated when added together at receiver 1 without considering the variation of amplitude and phase difference over the wide frequency band. The causes and effects resulting from the variation of amplitude and phase in wideband signals are analyzed in this section, and simulation results are provided.

In the 4 × 4 MIMO measurement system shown in Fig. 6, the MIMO test system comprises a minimum of four essential components, including a computer, testing instruments, a system control panel facilitating RF components and turntable control, and an integrated anechoic chamber. During the MIMO testing, the transmitting paths of testing signals are comprised of various active and passive components, such as the amplifier, filters, RF switches, measurement probes, RF cables, and propagation paths. All these components have a different impact on the amplitude and phase shift of the signals over the frequency band.

A. Amplitude Functional Variation

As illustrated above, many factors contribute to the amplitude flatness over the frequency band. Fig. 7 represents two primary cases: the amplitude of signals with linear functional variation and nonlinear functional variation. The first source spectrum line is the reference signal without amplitude variation, and the second line is amplitude-modulated after the propagation environment.

To implement the simulation and determine the effect of amplitude variations, two 5G new radio (NR) signals with different amplitude variations were added together in antiphase (180° difference) to analyze the canceled power levels at different bandwidths, and the results are shown in Fig. 8 and Table I. With the bandwidth and amplitude variation increase shown in Fig. 8, the canceled power level decreases after adding these two phase-reversed signals together, which would result in lower isolation for the RTS method and introduce MIMO measurement uncertainties. To improve the isolation (>15 dB) in different bandwidths, the maximum amplitude variation should be ensured as shown in Table I.

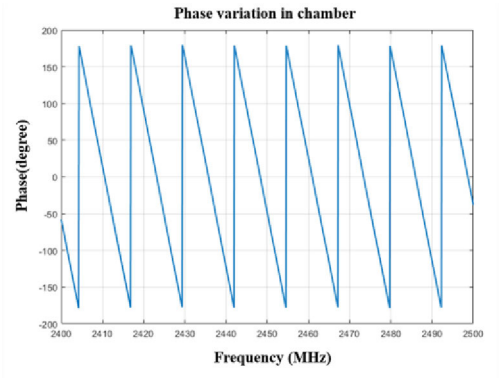

Fig. 9. Phase variation in a chamber for a communication link.

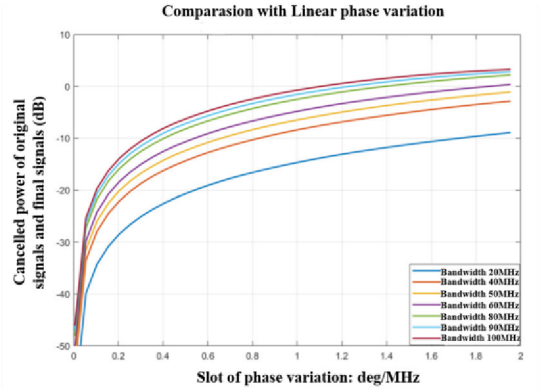

Fig. 10. Magnitude of power canceling in a different bandwidth and phase slop.

For 5G MIMO measurements with a 100-MHz bandwidth, it is difficult to guarantee the amplitude variation within 0.8 dB for individual RF components, let alone for an anechoic chamber design. Therefore, on the one hand, amplitude-flat components and low-loss cables for chamber design can be used to reduce the amplitude variation; on the other hand, the amplitude variation can also be addressed by the method introduced in Section IV.

B. Phase Variation

Unlike amplitude variation, phase variations with frequency can be significant in a complex communication link path. For example, assume that the attenuation of the RF cable can be ignored, the wavelength and the phase progression are

$$\lambda = \frac{2\pi}{\beta} = \frac{2\pi}{\omega\sqrt{\mu\epsilon}}$$

and

$$\varphi = \frac{l}{\lambda} = \frac{l\omega\sqrt{\mu\epsilon}}{2\pi} \tag{9}$$

where l is the cable length, ω is the radian frequency of the signals, and μ and ϵ represent the magnetic permeability and electrical permittivity, respectively. The variation of the phase with frequency is

$$\frac{\Delta\varphi}{\Delta\omega} = \frac{l\sqrt{\mu\epsilon}}{2\pi}. \tag{10}$$

The phase variation at 2.45 GHz with a 100-MHz signal bandwidth is simulated and shown in Fig. 9. As the frequency increases, the phase varies with the frequency, as well as the length of the total communication link, and the phase change from the amplifier, filter, and other RF components. To cancel the cross-link power shown in Fig. 5, the magnitude of the phase variation under a different frequency of the two signals should have the same trends and values to ensure that all the in-band frequencies can be adjusted for phase cancellation (180° difference). If not, even though the phase could be adjusted for cancellation at the center frequency, the phase at off-center frequencies is not canceled, thus resulting in a cross-link signal that is not eliminated at off-center frequencies.

The phase of the communication link is a very sensitive parameter, which is sensitive to the cable length, amplifier, filters, and even the performance of antennas. It is difficult to ensure that all communication links have the same phase variation. It is assumed that the two-communication links in Fig. 5 have a different slope of the phase, the canceled power level is simulated, and results are simulated and shown in Fig. 10. As the bandwidth and phase-slope difference increase, the ability of power cancellation decreases. When the slope of the phase difference is too large, the power level can even be increased. In a large chamber, the cable length can be significant (>100 m), and the RF components can be more complex, thus resulting in a more complex change of phase, as well as low isolation, and high MIMO measurement uncertainty.

IV. Solution

Amplitude and phase variations in the propagation environment bring challenges in wideband MIMO evaluation based on the RTS method. The traditional inverse matrix M in the RTS method is typically linearly adjusted without considering amplitude and phase variation in wideband signals. Therefore, the theoretical calculation and realization of the inverse matrix M must be improved to accommodate wideband OTA MIMO measurements.

A. Inverse Matrix M_W for Wideband Signals

The traditional inverse matrix M is calculated and applied based on the center frequency of the signals with narrow bandwidth (e.g., 4G LTE with 20-MHz-frequency bandwidth). However, this narrowband inverse matrix cannot be adapted to the wideband signals because of the amplitude and phase variations in the communication link. As shown in Figs. 7 and 9, with the amplitude and phase variation over frequency, the transmitting matrix H at the center frequency can vary over the total frequency band appreciably, thus resulting in an unsuitable inverse matrix. To realize the inverse matrix to cover the entire signal band, the wideband signal can be divided into several narrowband signals, and then, the inverse matrix calculated and applied in each narrowband to realize the wideband inverse matrix. The total wideband inverse matrix M_W is a mathematical transformation algorithm to adjust the amplitude and phase under different frequencies f to meet

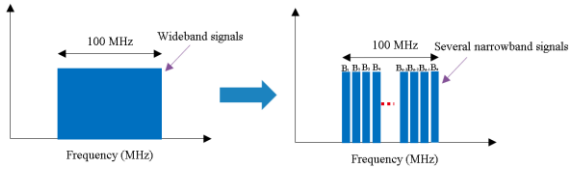

Fig. 11. Dividing the wideband signals.

the OTA chambers propagation environment. To realize the wideband inverse matrix, the discrete Fourier transform (DFT) and the inverse discrete Fourier transform (IDFT) are used in the signal processing. Hence, the calculation of wideband inverse matrix M_W can be divided into the following steps.

Step 1: Divide the wideband signals into n narrowband signals $B_1, B_2, \ldots, B_n$ (as shown in Fig. 11, signals with 100 MHz as an example). Each B_i was used for the transmitting matrix calculation, and the number of narrowband n is determined by the DFT length.

Step 2: Obtain the transmitting matrix $H_1, H_2, \ldots, H_n$ at the center frequency of $B_1, B_2, \ldots, B_n$, and then, calculate the inverse matrix $M_1, M_2, \ldots, M_n$ of each narrowband. The ith transmitting matrix H_i and the inverse matrix M_i for B_i are given as follows:

$$H_i = \begin{bmatrix} h_{i,11} & h_{i,12} \\ h_{i,21} & h_{i,22} \end{bmatrix}$$
$$M_i = \begin{bmatrix} m_{i,11} & m_{i,12} \\ m_{i,21} & m_{i,22} \end{bmatrix} \tag{11}$$

where for narrowband signals, the $H_i \approx H_{(n/2)}$ ($H_{(n/2)}$ represents the transmitting matrix at the center frequency), so the inverse matrix at the center frequency is adapted to the tested band. However, as the bandwidth increases, the H_i and M_i varies with frequency significantly, and the amplitude and phase variation would be reflected in H_i. Hence, the M_W is the function of frequency which could be written as

$$M_W(f) = \begin{bmatrix} m_{1,1}'(f) & \cdots & m_{1,N}'(f) \\ \vdots & \ddots & \vdots \\ m_{N,1}'(f) & \cdots & m_{N,N}'(f) \end{bmatrix} \tag{12}$$

where $m_{j,k}'(f)$ is composed of $m_{1,jk}, m_{2,jk}, \ldots, m_{n,jk}$, where j and k equal to 1 or 2 in 2×2 MIMO systems.

Step 3: Convert the desired signals in $m_{j,k}'$ communication link from time domain to frequency domain using a DFT

$$X_{j,k}(w) = \sum_{n=0}^{N-1} x_{j,k}(n) e^{-j\frac{2\pi wn}{N}} \tag{13}$$

where $x(n)$ is the discrete signal of $x(t)$, N is the DFT length (usually $N = 8, 16, 32, 64, 128, 256, 512$, or 1024), and $X(n)$ is the frequency-domain value of $x(n)$.

Step 4: Calculate the output signals of the $m_{j,k}'$ communication link for the wideband matrix M_W over different frequencies. The calculated value in the frequency domain is

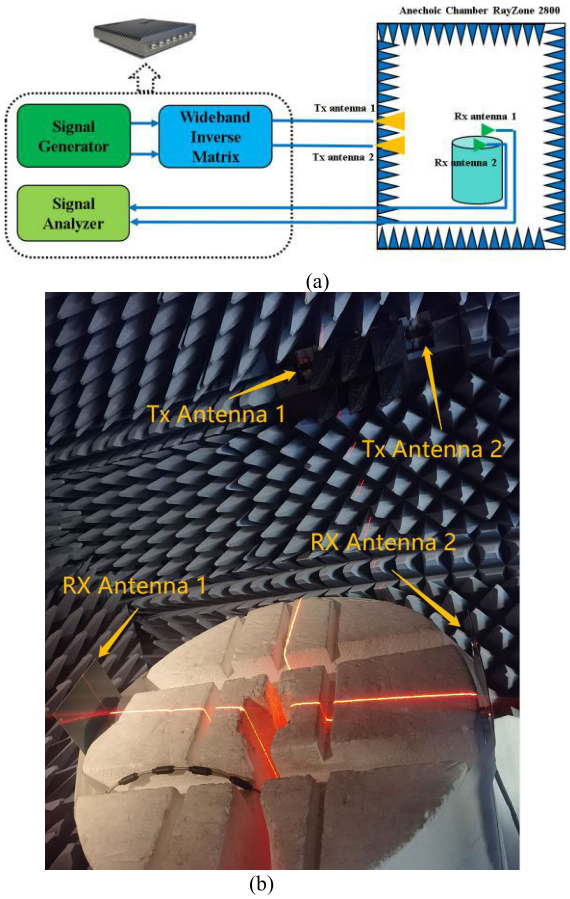

Fig. 12. Measurement schematic and setup to represent a 2×2 MIMO system: (a) schematic of a 2×2 MIMO system and (b) measurement setup.

represented as

$$X_{j,k}'(w) = X_{j,k}(w) m_{j,k}'(f). \tag{14}$$

Step 5: Convert the calibrated value from frequency domain to time domain using an IDFT, so the calculated signal in the wideband inverse matrix is written as

$$x_{j,k}'(n) = \sum_{w=0}^{N-1} X_{j,k}'(w) e^{j\frac{2\pi nw}{N}}. \tag{15}$$

Step 6: The transmitting signals for Tx antenna j are then

$$Tx_j = \sum_{k=1}^{k=N} x_{j,k}'(n). \tag{16}$$

Applying the wideband inverse matrix, M_W, and the DFT/IDFT algorithm to the RTS MIMO measurement, the amplitude and phase variation can be calibrated and canceled to achieve higher isolation for wideband signals, as well as improving the measurement accuracy in 5G MIMO measurements. In addition, the wideband inverse matrix M_W algorithm can only be applied by DSP or FPGA on baseband data in instruments instead of RF components because the wide frequency band is "sliced" into individual narrower bands, and the RF components are difficult to adjuste to adapt to such wideband signals.

V. Validation

A. Measurement Setup and Steps

To verify the wideband inverse matrix algorithm, a measurement setup is constructed as shown in Fig. 12. Two transmitting antennas and two receiving antennas are placed in the anechoic chamber to simulate the antenna isolation for 2×2 MIMO systems. In addition, a vector signal generator/analyzer and the wideband inverse matrix algorithm are integrated into an instrument to transmit the desired signals, analyze the receiving signals, and verify the algorithm. The instrument, the ODC200, produced by General Test System Inc., Nanshan Dist., Shenzhen has multiple RF ports that can be configured as either transmitters or receivers. For the verification process, two ports are assigned to transmitting antennas and the other two ports are assigned to receiving antennas, as shown in Fig. 12(a). The wideband inverse algorithm is integrated into a single module within the ODC200, and the relevant parameters can be readily imported into this module before transmitting the wideband signals. Moreover, the measurement procedures are executed as follows.

1) Position the transmitting and receiving antennas within an anechoic chamber to simulate the transmitter of the testing instrument and the receiver of the DUT.
2) Choose signals with different bandwidths of the frequency range of interest and divide the wideband signal into several narrowband subsignals, ranging from 8 to 128 or greater.
3) Transmit continuous waves at the center frequency of each narrowband subsignal from multiple transmit antennas and receive the signals using multiple receiving antennas to obtain the spatial complex transmission matrix H for the transmitter and receiver.
4) Calculate the inverse matrix of each narrowband subsignal and apply these parameters to the wideband inverse matrix module using (12)–(16). Generate the output time-domain signal, and transmit it through the transmit antennas.
5) Configure the signal generator with a wideband signal and activate either transmitter 1 or transmitter 2. After applying the wideband inverse matrix, measure the power received by receiver 1 and receiver 2, and calculate the antenna isolation for both scenarios.
6) Apply the inverse matrix of the center frequency point to the wideband inverse matrix module, calculate the output time-domain signal, and transmit it through the transmitting antenna.
7) Repeat step (5) to obtain the antenna isolations.
8) Compare the spectrum and isolation results obtained using the wideband inverse matrix from step (5) and the narrowband inverse matrix at the center frequency from step (7).
9) Configure various bandwidths and repeat steps (2)–(8).

B. Measurement Results

In this measurement, the frequencies 2.45 and 4.95 GHz are selected as the center frequency with a maximum bandwidth of 100 MHz to verify the algorithm.

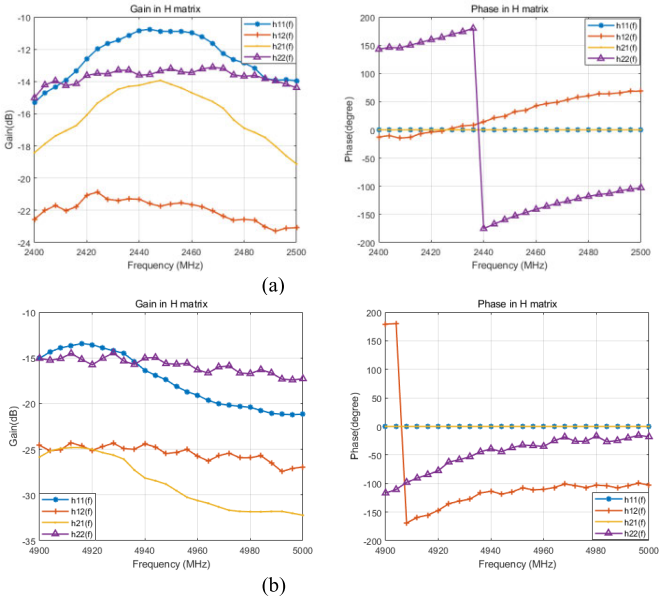

Fig. 13. H-matrix with center frequencies of: (a) 2.45 and (b) 4.95 GHz with 100-MHz bandwidth.

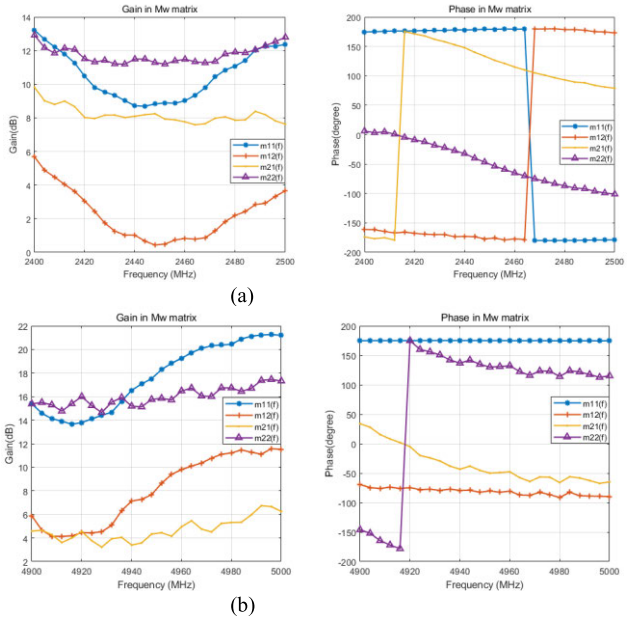

Fig. 14. M_W-matrix for: (a) 2.45 and (b) 4.95 GHz with 100-MHz bandwidth.

As shown in Fig. 13, due to the existence of the cables, amplifier, filter, and attenuator, the maximum amplitude and phase variation over the 100-MHz bandwidth is over 4 dB and 70° in 2.45 GHz and more significant over the 4.95-GHz range. In addition, it should be noted that the observed discontinuity in phase change, as presented in Figs. 13 and 14, is attributed to the normalization of the phase results within the range of −180° to 180°.

As shown in Fig. 14, the adjusted amplitude and phase vary with the frequency in the wideband inverse matrix. The adjusted amplitude/phase reaches nearly the maximum of 5 dB/100° in the 2.45-GHz center frequency case and 8 dB/100° in the 4.95-GHz center frequency case over the

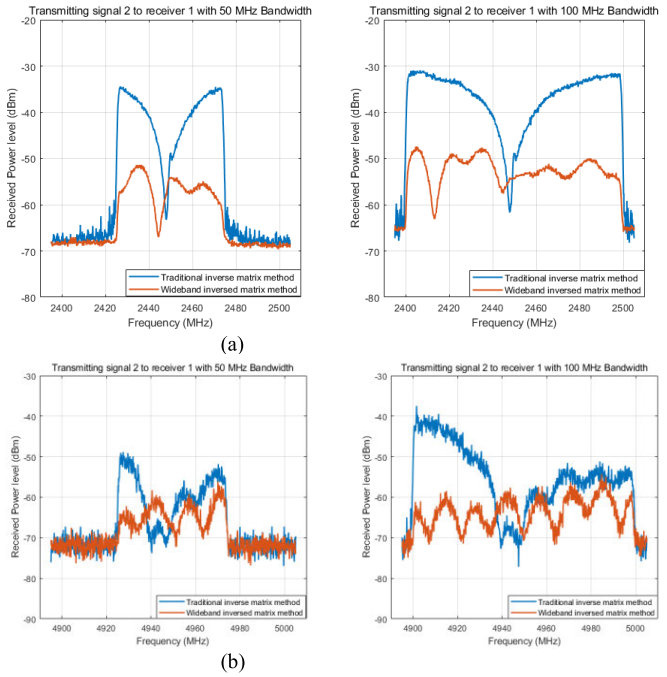

Fig. 15. Spectrum for 2.45 and 4.95 GHz with 100-MHz bandwidth: (a) spectrum for 2.45 GHz with 50- and 100-MHz bandwidths and (b) spectrum for 4.95 GHz with 50- and 100-MHz bandwidths.

TABLE II
ANTENNA ISOLATIONS COMPARISON IN 2.45 AND 4.95 GHZ

Center Freq (MHz)	Bandwidth (MHz)	Traditional Method			Proposed Method		
		Ios_1	Ios_2	Ios_t	Ios_1	Ios_2	Ios_t
2450	20	21.1	26.8	21.1	33.8	33	33
	40	15.7	21.7	15.7	33.8	34.9	33.8
	50	13.9	20.3	13.9	34	35.2	34
	60	12.5	18.9	12.5	33.7	35.8	33.7
	80	10.7	17.2	10.7	32.5	36.1	32.5
	90	9.9	16.5	9.9	31.8	36.3	31.8
	100	9.2	15.9	9.2	31	36.6	31
4950	20	24.7	24.2	24.2	29.1	28.5	28.5
	40	23.4	23	23	30.8	29.8	29.8
	50	21.8	21	21	30.4	30.6	30.4
	60	20.4	19.4	19.4	30.8	31.1	30.8
	80	17.5	15.9	15.9	30.3	31.8	30.3
	90	16.4	14.6	14.6	30.4	31.93	30.4
	100	15.4	13.8	13.8	30.5	32	30.5

total 100-MHz bandwidth. However, for 4G LTE with a 20-MHz bandwidth in the center frequency, this adjusted amplitude/phase is reduced to 1 dB/30° in the 2.45-GHz center frequency case and 3 dB/10° in the 4.95-GHz center frequency case, which means that the inverse matrix at the center frequency is not suitable for the wideband signals.

As illustrated in Fig. 15, transmitting signal 2 to receiver 1 is taken as an example. After applying the inverse matrix, the ideal case is that the signals are canceled or significantly reduced. As shown in Fig. 15, the traditional inverse matrix considers only the center frequency of the signal band; therefore, based on the spectral analysis of the results, it was found that the power cancellation effect of the wideband signal is most effective at the center frequency due to the utilization of transmission and inverse matrices at this frequency. However, this approach is not effective for signals located far from the center frequency when the bandwidth is expanded, which ultimately presents a challenge in enhancing the final antenna isolation. After applying the proposed wideband inverse matrix algorithm, the power across the entire signal bandwidth is significantly reduced, thus leading to improved antenna isolation in OTA MIMO systems.

As shown in Table II, the antenna isolation decreases as the bandwidth increases using the traditional method with the inverse matrix at the center frequency. When it comes to the 100-MHz bandwidth, the antenna isolation is reduced to less than 15 dB, thus resulting in high MIMO measurement uncertainty. However, the antenna isolation is vastly improved to greater than 25 dB using the proposed method.

VI. CONCLUSION

With the rapid developments for 5G wireless systems, the OTA measurement has become the most efficient method to evaluate the transceiver performance of a DUT. As one of the critical aspects of performance evaluation, the MIMO OTA measurement should reflect the actual usage performance for MIMO devices with the increased bandwidth in 5G communications. As the bandwidth of 5G signals increases (sub-6 GHz reaches a maximum of 100 MHz in a single-frequency bandwidth; mm-wave reaches a maximum of 400 MHz), the functional variation of amplitude and phase is increased, which results in lower antenna isolation in the RTS OTA MIMO evaluation because the traditional inverse matrix method can only be adapted to narrowband signals with small amplitude and phase variation.

A wideband inverse matrix is proposed herein to solve the RTS MIMO measurement for wideband signals. The frequency in the wideband signals is divided into several narrowband slices, and the transmitting matrix H and inverse matrix M are obtained and calculated in each part. Finally, the signals are calculated using the total wideband inverse matrix Mw, DFT, and IDFT method [in (11)–(15)] to obtain the final desired transmitting signals.

After applying the wideband inverse matrix algorithm to the MIMO system, the antenna isolations are improved significantly (>25 dB in 100-MHz bandwidth) to reduce the MIMO measurement uncertainty. The proposed algorithms can be applied to both uplink and downlink MIMO measurements when the transmitting matrix and its wideband inverse matrix are measured. For MIMO measurements with carrier aggregation (CA), the frequency carriers can be divided into several single carriers using filters, and the wideband matrix can be calculated and applied to each frequency carrier. The output signals can then be combined for MIMO evaluations to realize RTS MIMO measurements with CA. In addition, this calculation process and algorithm can also be used in the MPAC method to handle the amplitude and phase variation in the chamber. This article paves the way for engineers to correctly evaluate the MIMO

performance in wideband signals and reduce the measurement uncertainty.

REFERENCES

[1] A. Yarali, "AI, 5G, and IoT," in *Intelligent Connectivity: AI, IoT, and 5G*. Hoboken, NJ, USA: Wiley, 2022, pp. 117–131. [Online]. Available: https://onlinelibrary.wiley.com/doi/book/10.1002/9781119685265#about Book-pane, doi: 10.1002/9781119685265.ch6.

[2] Y. Qi et al., "5G Over-the-air measurement challenges: Overview," *IEEE Trans. Electromagn. Compat.*, vol. 59, no. 6, pp. 1661–1670, Dec. 2017, doi: 10.1109/TEMC.2017.2707471.

[3] Y. Jing, M. Rumney, H. Kong, and Z. Wen, "Overview of 5G UE OTA performance test challenges and methods," in *IEEE MTT-S Int. Microw. Symp. Dig.*, May 2018, pp. 1–4, doi: 10.1109/IEEE-IWS.2018.8400996.

[4] *Everything Wireless*. [Online]. Available: http://www.ctia.org

[5] *Universal Mobile Telecommunications System (UMTS); LTE; Universal Terrestrial Radio Access (UTRA) and Evolved Universal Terrestrial Radio Access (E-UTRA); Verification of Radiated Multi-Antenna Reception Performance of User Equipment (UE)*, ETSI, Sophia Antipolis, France, document 37.977, V12.0.0, 3GPP, 2017.

[6] P. Shen, Y. Qi, J. Fan, and Y. Wang, "The advantages of the RTS method in MIMO OTA measurements," in *Proc. IEEE Int. Symp. Electromagn. Compat. Signal/Power Integrity (EMCSI)*, Aug. 2017, pp. 470–473, doi: 10.1109/ISEMC.2017.8077916.

[7] P. Shen, Y. Qi, W. Yu, and F. Li, "Inverse matrix autosearch technique for the RTS MIMO OTA test," *IEEE Trans. Electromagn. Compat.*, vol. 63, no. 4, pp. 962–969, Aug. 2021, doi: 10.1109/TEMC.2020.3029909.

[8] Y. Jing, H. Kong, and M. Rumney, "MIMO OTA test for a mobile station performance evaluation," *IEEE Instrum. Meas. Mag.*, vol. 19, no. 3, pp. 43–50, Jun. 2016, doi: 10.1109/MIM.2016.7477954.

[9] W. Yu, Y. Qi, K. Liu, Y. Xu, and J. Fan, "Radiated two-stage method for LTE MIMO user equipment performance evaluation," *IEEE Trans. Electromagn. Compat.*, vol. 56, no. 6, pp. 1691–1696, Dec. 2014, doi: 10.1109/TEMC.2014.2320779.

[10] Y. Jing, T. Hertel, H. Kong, P. Shen, and Y. Liu, "Recent developments in radiated two-stage MIMO OTA test method," in *Proc. 14th Eur. Conf. Antennas Propag. (EuCAP)*, Mar. 2020, pp. 1–5, doi: 10.23919/EuCAP48036.2020.9135252.

[11] J. Li, Y. Qi, and J. Fan, "Over-the-air measurement for MIMO systems," *Frontiers Inf. Technol. Electron. Eng.*, vol. 22, no. 8, pp. 1046–1058, Aug. 2021.

[12] P. Shen, Y. Qi, W. Yu, J. L. Drewniak, M. Yu, and F. Li, "An RTS-based near-field MIMO measurement solution—A step toward 5G," *IEEE Trans. Microw. Theory Techn.*, vol. 67, no. 7, pp. 2884–2893, Jul. 2019, doi: 10.1109/TMTT.2019.2901687.

[13] Y. Jing, H. Kong, and M. Rumney, "Radiated two-stage MIMO OTA test method progress for antenna performance evaluation," in *Proc. Asia–Pacific Int. Symp. Electromagn. Compat. (APEMC)*, May 2016, pp. 729–731.

[14] P. Shen, Y. Qi, W. Yu, J. Fan, and F. Li, "OTA measurement for IoT wireless device performance evaluation: Challenges and solutions," *IEEE Internet Things J.*, vol. 6, no. 1, pp. 1223–1237, Feb. 2019, doi: 10.1109/JIOT.2018.2868787.

[15] Y. Wang, S. Wu, Z. Yang, P. Shen, C. Wu, and J. Fan, "MIMO performance diagnosis based on the radiated two-stage (RTS) method," in *Proc. IEEE Symp. Electromagn. Compat., Signal Integrity Power Integrity*, Jul. 2018, pp. 489–492.

[16] P. Shen, Y. Qi, W. Yu, J. Fan, Z. Yang, and S. Wu, "A decomposition method for MIMO OTA performance evaluation," *IEEE Trans. Veh. Technol.*, vol. 67, no. 9, pp. 8184–8191, Sep. 2018, doi: 10.1109/TVT.2018.2839726.

[17] *User Equipment (UE) Over the Air (OTA) Performance; Conformance Sting*, document TS 37.544 V14.5.0, 3GPP, 2018.

[18] J. Li et al., "Temperature effects in OTA MIMO measurement," *IEEE Trans. Instrum. Meas.*, vol. 70, pp. 1–9, 2021, doi: 10.1109/TIM.2020.3014005.

[19] P. Shen, Y. Qi, W. Yu, and J. Fan, "UE reporting uncertainty analysis in radiated two-stage MIMO measurements," *IEEE Trans. Antennas Propag.*, vol. 69, no. 12, pp. 8808–8815, Dec. 2021, doi: 10.1109/TAP.2021.3090523.

Jun Li (Student Member, IEEE) received the B.S. and M.S. degrees in electronic information and technology from Hunan University, Changsha, China, in 2016 and 2019, respectively. He is currently pursuing the Ph.D. degree in information and communications engineering with Dalian Maritime University, Dalian, China.

His research interests include single-input single-output (SISO) and multiple-input multiple-output (MIMO) measurements for wireless devices, as well as microwave and RF hardware design.

Bin Lin (Senior Member, IEEE) received the B.S. and M.S. degrees from Dalian Maritime University, Dalian, China, in 1999 and 2003, respectively, and the Ph.D. degree from the Broadband Communications Research Group, Department of Electrical and Computer Engineering, University of Waterloo, Waterloo, ON, Canada, in 2009.

She was a Visiting Scholar with The George Washington University, Washington, DC, USA, from 2015 to 2016. She is currently a Full Professor and the Dean of the Communication Engineering Department, School of Information Science and Technology, Dalian Maritime University. She is also a Scientist with the Peng Cheng Laboratory, Shenzhen, China. Her current research interests include wireless communications, network dimensioning and optimization, resource allocation, artificial intelligence, maritime communication networks, edge/cloud computing, wireless sensor networks, and Internet of Things.

Dr. Lin is an Associate Editor of the Institution of Engineering and Technology (IET) Communications.

Yihong Qi (Fellow, IEEE) received the B.S. degree in electronics from the National University of Defense Technologies, Changsha, China, in 1982, the M.S. degree in electronics from the Chinese Academy of Space Technology, Beijing, China, in 1985, and the Ph.D. degree in electronics from Xidian University, Xi'an, China, in 1989.

From 1989 to 1993, he was a Post-Doctoral Fellow and then an Associate Professor with Southeast University, Nanjing, China. From 1993 to 1995, he was a Post-Doctoral Researcher with McMaster University, Hamilton, ON, Canada. From 1995 to 2010, he was with Research in Motion (Blackberry), Waterloo, ON, where he was the Director of Advanced Electromagnetic Research. He is currently a Scientist with the Peng Cheng Laboratory, Shenzhen, China, and the President and the Chief Scientist with General Test Systems, Inc., Shenzhen. He founded DBJay, Zhuhai, China, in 2011. He is also an Adjunct Professor with the EMC Laboratory, Missouri University of Science and Technology, Rolla, MO, USA; Western University, London, ON; and Hunan University, Changsha, and an Honorary Professor with Southwest Jiaotong University, Chengdu, China. He is an inventor of more than 450 published and pending patents.

Dr. Qi has received the IEEE EMC Society Technical Achievement Award in August 2017. He was a Distinguished Lecturer of the IEEE EMC Society for 2014 and 2015, and the Founding man of the IEEE EMC TC-12. He is a fellow of the Canadian Academy of Engineering and National Academy of Inventors.

James L. Drewniak (Fellow, IEEE) received the B.S., M.S., and Ph.D. degrees in electrical engineering from the University of Illinois at Urbana–Champaign, Champaign, IL, USA, in 1985, 1987, and 1991, respectively.

He is currently a Curator's Professor Emeritus with the Missouri University of Science and Technology (Missouri S&T), Rolla, MO, USA.

Jiang Zhu (Fellow, IEEE) received the B.S. degree in information science and electronic engineering from Zhejiang University, Hangzhou, China, in 2003, the M.A.Sc. degree in electrical engineering from McMaster University, Hamilton, ON, Canada, in 2006, and the Ph.D. degree in electrical engineering from the University of Toronto, Toronto, ON, in 2010.

From 2010 to 2014, he was a Senior Hardware Engineer with Apple Inc., Cupertino, CA, USA. From 2014 to 2016, he was with the Google[x] Life Science Division and then a Founding Member with Verily Life Science, a subsidiary of Alphabet Inc., Mountain View, CA, USA. From 2016 to 2021, he founded the Wearable Wireless Hardware Group, Google LLC, Mountain View, and led the antenna and RF research and development for the emerging wrist-worn, hearable, virtual reality, and augmented reality products, projects, and technologies. In 2021, he joined the Meta Reality Labs, Sunnyvale, CA, USA, as the Head of Antenna Research, where he leads a group of talented and diverse research scientists and engineers working on the enabling technologies for the immersive wearable computing. His work leads to over 100 IEEE journal and conference publications and U.S. patents, many of them have been commercialized in some of the most popular consumer products in the world. His research interests are the consumer applications of RF, antennas, and electromagnetics in the areas of wireless communications, human body interaction and sensing, and wireless power.

Dr. Zhu was a recipient of the IEEE Microwave Theory and Techniques Society Outstanding Young Engineer Award and the IEEE Antennas and Propagation Society Doctoral Research Award. He has received several student paper awards as a student as well as a Project Supervisor, including the most recent one—the First Place Best Student Paper Award in the 2021 IEEE AP-S Symposium on Antennas and Propagation with his Intern Student at Google. He serves as the TPC Chair for the 2023 IEEE International Workshop on Antenna Technology and the TPC Co-Chair for the 2022 IEEE International Microwave Biomedical Conference. He serves on TPC and TPRC for numerous conferences, including IEEE APS, IMS, and RWS. He is a Senior Editor of the IEEE OPEN JOURNAL OF ANTENNAS AND PROPAGATION and an Associate Editor of the IEEE TRANSACTIONS ON ANTENNAS AND PROPAGATION, the IEEE INTERNET OF THINGS JOURNAL, the IEEE ANTENNAS AND WIRELESS PROPAGATION LETTERS, and *IET Microwaves, Antennas, & Propagation*. He is also the Guest Co-Editor of the *IEEE Communications Magazine*—Special Feature Topic on Antenna Systems for 5G and Beyond, and the IEEE OPEN JOURNAL OF ANTENNAS AND PROPAGATION—Special Section on Advances in Antenna Design for Metaverse and Other Modern Smart Mobile Devices. He is a member of the IEEE AP-S Industrial Initiatives Committee, the IEEE AP-S Young Professional Committee, the IEEE MTT-S Technical Coordination Future Directions Committee—IoT Working Group, and the IEEE MTT-26 RFID, Wireless Sensors, and IoT Committee. He is a member and an Industry Liaison of the IEEE AP-S Membership and Benefits Committee.

Daryl G. Beetner (Senior Member, IEEE) received the B.S. degree from Southern Illinois University, Edwardsville, IL, USA, in 1990, and the M.S. and D.Sc. degrees from Washington University, St. Louis, MO, USA, in 1994 and 1997, respectively, all in electrical engineering.

He is currently a Professor of Electrical and Computer Engineering with the Missouri University of Science and Technology (Missouri S&T), Rolla, MO, where he is also the former Chair of the ECE Department, the Director of the Electromagnetic Compatibility Laboratory, and the Director of the Center for Electromagnetic Compatibility, a National Science Foundation Industry/University Cooperative Research Center. His research interests include electromagnetic immunity and emissions from the integrated circuit to the system level.